Development and Proof-of-Concept of Three-dimensional Lung Histology Volumes

Lindsay Mathew[1], Mostafa Alabousi[1], Andrew Wheatley[1], Usaf Aladl[1], Deborah Slipetz[2], James C Hogg[3], Aaron Fenster[1] and Grace Parraga[1]

1. Imaging Research Laboratories, Robarts Research Institute, London, Canada;

2. Merck Research Laboratories, Montreal Canada

3. The James Hogg Research Centre, University of British Columbia and St. Paul's Hospital, Vancouver, Canada

Most medical imaging is inherently three-dimensional (3D) but for validation of pathological findings, histopathology is commonly used and typically histopathology images are acquired as two-dimensional slices with quantitative analysis performed in a single dimension. Histopathology is invasive, labour-intensive, and the analysis cannot be performed in real time, yet it remains the gold standard for the pathological diagnosis and validation of clinical or radiological diagnoses of disease. A major goal worldwide is to improve medical imaging resolution, sensitivity and specificity to better guide therapy and biopsy and to one day delay or replace biopsy. A key limitation however is the lack of tools to directly compare 3D macroscopic imaging acquired in patients with histopathology findings, typically provided in a single dimension (1D) or in two dimensions (2D). To directly address this, we developed methods for 2D histology slice visualization/registration to generate 3D volumes and quantified tissue components in the 3D volume for direct comparison to volumetric micro-CT and clinical CT. We used the elastase-instilled mouse emphysema lung model to evaluate our methods with murine lungs sectioned (5 μm thickness/10 μm gap) and digitized with 2μm in-plane resolution. 3D volumes were generated for wildtype and elastase mouse lung sections after semi-automated registration of all tissue slices. The 1D mean linear intercept (L_m) for wildtype (WT) (47.1 μm ± 9.8 μm) and elastase mouse lung (64.5 μm ± 14.0 μm) was significantly different ($p<.001$). We also generated 3D measurements based on tissue and airspace morphometry from the 3D volumes and all of these were significantly different ($p<.0001$) when comparing elastase and WT mouse lung. The ratio of the airspace-to-lung volume for the entire lung volume was also significantly and strongly correlated with L_m.

Description of Purpose:

Three dimensional imaging tools, such as magnetic resonance imaging (MRI) and x-ray computed Tomography (CT) provide a way to quantitatively evaluate emphysema and measurements made using these tools can be directly compared to tissue pathology samples – the gold standard method for evaluating emphysema. The goal of this work was to develop image processing tools for the generation and manipulation of three-dimensional mouse lung histology volumes providing high resolution three-dimensional images of lung parenchyma tissue and airways. In this proof of concept study, the well-established elastase mouse model was used for comparison to WT mice.

Methods:

Lung Tissue Processing

Male C57BL/6 mice (20-25 gram body weight, Charles River Canada) were anesthetized (3% isoflurane) and received either 3U of porcine pancreatic elastase (PPE, Elastin Product Company #EC134) in 30 μl of 0.9% saline or 30 μl of saline by intratracheal instillation. Briefly, a mid-line incision was made on the neck, the trachea exposed, and a 22 gauge Cathlon catheter was inserted (1 cm) into the trachea between two tracheal rings. PPE or saline was slowly injected into trachea.

Medical Imaging 2012: Biomedical Applications in Molecular, Structural, and Functional Imaging, edited by Robert C. Molthen, John B. Weaver, Proc. of SPIE Vol. 8317, 83171N · © 2012 SPIE · CCC code: 1605-7422/12/$18
doi: 10.1117/12.912620

After instillation of PPE or saline, a syringe bulb was attached to the needle and each mouse received two puffs of air into their lungs. The skin incision was closed via a single staple after application of iodine, alcohol and 0.025% bupivacane to skin edges. Mice were allowed to recover from surgery in a heated box (37°C) for 10 minutes. Animal weights were taken 4 times per week until the end of the study. Clinical observations were made daily to assess the welfare of the animals during the study. Two weeks after elastase or vehicle treatment, mice were euthanized with an overdose of sodium pentobarbital (10 mg/mouse ip). The heart, trachea and both lungs were removed *en toto*. The lungs were externally rinsed and placed on a moistened paper towel. The trachea was cannulated with a 25-guage catheter which was securely attached via surgical thread. Lungs were infused with 60 ml of saline using a syringe pump system to rinse blood from lungs. Lungs were then infused with 5% buffered formalin solution for 30 minutes at 25 mmHg pressure to maximally inflate the lungs, after which the whole lung structure was placed in 5% buffered formalin until further processing. The lungs remained attached to the heart in order to preserve the natural anatomical alignment and embedded in paraffin wax overnight (Leica ASP 300, Leica Microsystems, Concordia ON). Tissue was sliced with 5 µm thickness (Microm HM 335 E Apogent Technologies, Portsmouth NH) and 10µm gap. The slices were placed in a hotbath and mounted on slides. After being placed in the oven over night (internal temperature 37 °C), the slides were stained with a Leica Autostainer XL (Leica Microsystems) using Hematoxylin and Eosin (H&E) stain sequence. These slides were digitized using a TissueScope T2-b scanner (Huron Technologies International Inc., Waterloo ON) with an in-plane resolution of 2µm.

Image Registration and Segmentation

Each image was registered using custom-built software (HToolKit, Robarts Research Institute, London ON) generated using the VTK Tool kit. Registration was based on the similarity measure that was used to correctly align the source image to the target image. We used a normalized cross-correlation metric where the cross-correlation ***s*** of a source image with the target image is given by:

$$s = \frac{\Sigma_i^n g(x_i) f(x_i)}{\sqrt{\Sigma_i^n g^2(x_i) \Sigma_i^n f^2(x_i)}}$$

where **g** is the target image and **f** is the source image. The similarity measure represents the value of the cost function value to be optimized over the search in the parameter space defined by rotation and xy translation. The Amoeba technique or the downhill simplex as proposed by Nelder and Mead (1) was used as the optimizer. This approach was used as it requires only function evaluations and not the derivatives of the function. Prior to the registration stage, all color images with 3 channels (RGB) were converted to gray by calculating a luminance from RGB values.

As shown in schematic in Figure 1, image slices were first padded to generate images of a standard size by lining their edges with black pixels, facilitating registration. To pad the slices, each image was centered and superimposed onto a black background 5% larger than the largest image in the set. To register all slices, user-defined translations and rotations of each digital slice were used for contiguous image slices. The coordinates of the transformations for the image registration were

generated and applied to the stack of approximately 250 slices or images. Following registration, the images were segmented to remove the background using a multi-threshold (2) with 3 clusters.

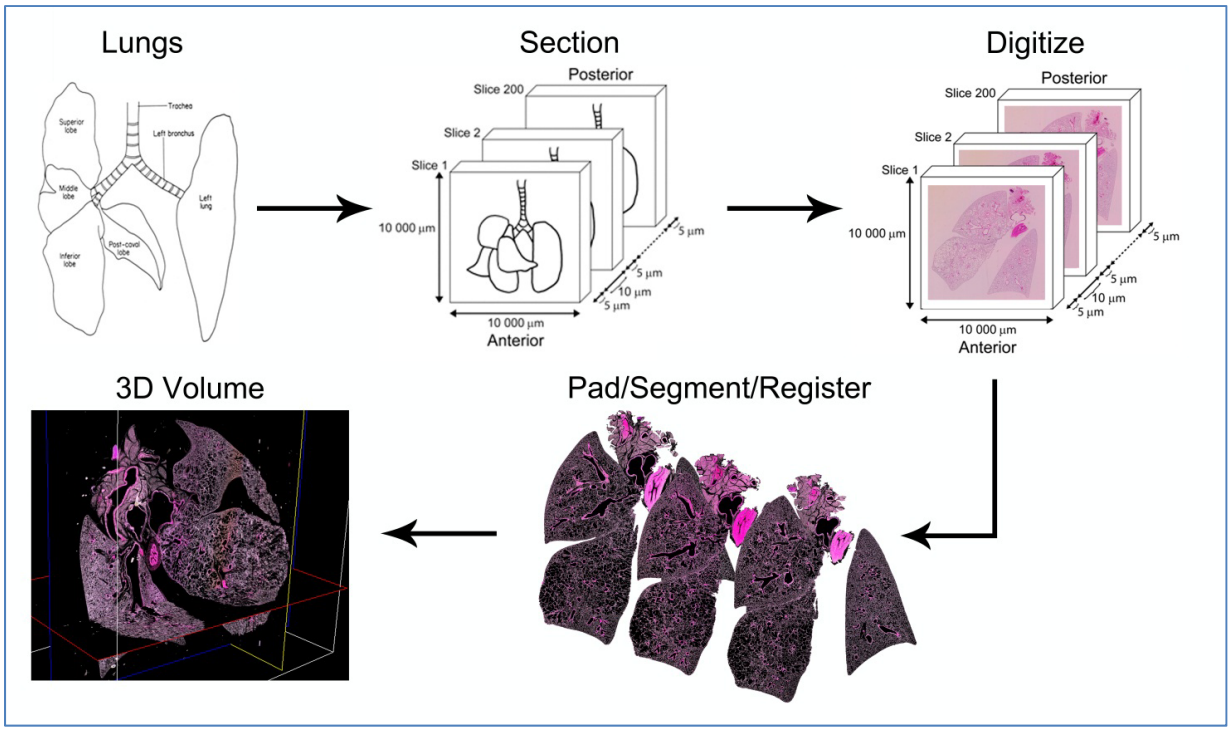

Figure 1. Schematic description of Murine lung 3D Histology Generation.
Steps 1-2: Mouse lungs were harvested inflated and tissue slices were prepared. Digital images were acquired with 2x2 um resolution using the Tissue-Scope scanner. Steps 3-5: The resultant digital images were padded, registered and the final 3D volume generated.

2D and 3D Lung Measurements

L_M measurements were generated using the stratified uniform random sampling (stURS) approach as outlined by the American Thoracic Society. Two regions in each of the five lobes across 5 sections of the lung were sampled for a total of 100 probe interactions for each set of lungs. We also developed a semi-automated method in MATLAB to generate L_M. A dynamic grid was superimposed on each section selected for sampling. Markers were placed automatically on edges defined as pixels with +1 intensity (black) that were adjacent to at least one non-black pixel. 3D measurements of total lung volume, total tissue volume, total airspace volume, and the airspace to volume ratio were evaluated for each lobe and total lung. To generate tissue volume measurements, the total number of voxels reporting tissue for each slice was multiplied by the slice thickness. Total lung volume was generated by applying a closing algorithm with a structural element of size 15, and then applying a filling algorithm to include areas within the closed region, creating a lung mask for each slice and multiplying each slice by its thickness.

Results:

Figure 2 shows a representative 3D histology volume composed of approximately 250 images slices generated using the method we developed. Although the method incorporates volume averaging over an apparent 15 μm slice, registration of the slices was sufficient to generate volumes that could be manipulated in the axial, coronal and sagittal planes.

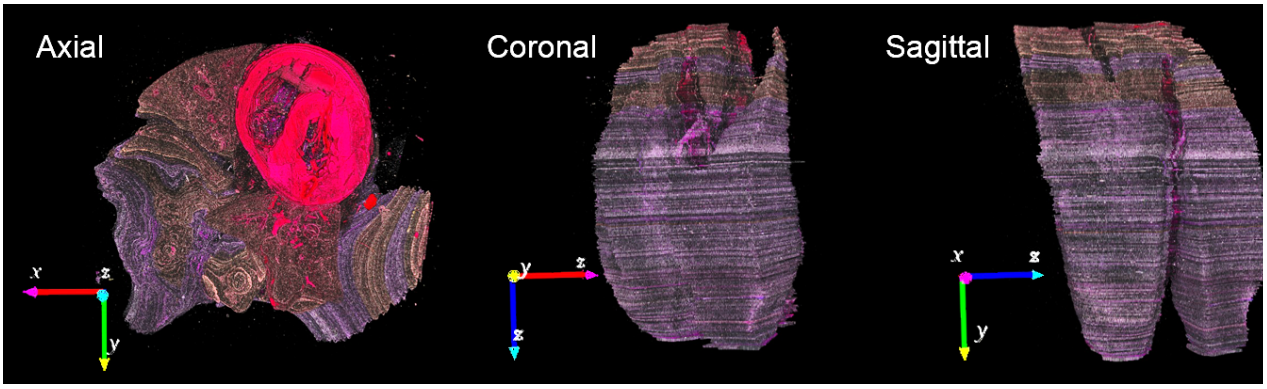

Figure 2. Final 3D histology volume generated from digitized slides of H&E stained, segmented, elastase mouse lungs shown in the axial, coronal and sagittal planes.

Table 1 shows the mean and standard deviation for L_M and volume measurements for elastase and wild-type lungs by lobe. L_M was significantly different between elastase and WT lungs ($p<0.001$). L_M was not significantly different between lobes of the wild-type lungs. ANOVA also indicated that L_M of right lobe 2 of the elastase-induced lungs was significantly different than the left lobe ($p<0.001$) and right lobe 1 ($p<0.05$).

Table 1. L_M and volumetric measurements for Wild-type and Elastase Lungs *p<.001 ** p<.0001

	Left Lobe	Right Lobe 1	Right Lobe 2	Right Lobe 3	Right Lobe 4	Total
L_M (μm)						
Wildtype	45.7 ± 8.5	45.0 ± 6.3	47.0 ± 9.7	49.3 ± 13.1	48.6 ± 11.4	47.1 ± 9.8*
Elastase	52.0 ± 7.9	61.3 ± 13.6	79.2 ± 9.6	63.9 ± 10.6	65.8 ± 13.8	64.5 ± 14.0*
Total Lung Volume (mm^3)						
Wildtype	51.8	42.4	28.4	14.9	1.5	139.0**
Elastase	53.7	36.0	80.6	19.1	13.3	202.7**
Tissue Lung Volume (mm^3)						
Wildtype	13.7	10.9	8.4	4.6	3.9	41.5**
Elastase	15.8	9.6	18.0	3.9	2.7	49.8**
Airspace Volume (mm^3)						
Wildtype	38.1	29.8	20.9	10.4	1.1	101.2**
Elastase	38.0	26.3	62.8	14.9	10.6	153.8**
Airspace:Lung Volume %						
Wildtype	73.5 ± 5.8	70.2 ± 6.3	73.7 ± 5.3	69.5 ± 6.1	73.7 ± 5.7	72.8 ± 5.2**
Elastase	70.7 ± 5.8	73.0 ± 5.8	77.9 ± 4.5	77.9 ± 7.0	79.8 ± 5.2	75.9 ± 5.6**
Tissue:Airspace Volume %						
Wildtype	37.1 ± 15.5	36.5 ± 11.3	44.1 ± 19.7	45.2 ± 16.8	36.6 ± 12.9	38.3 ± 13.2**
Elastase	42.4 ± 13.8	37.6 ± 10.4	28.7 ± 7.8	29.5 ± 12.6	25.9 ± 9.2	32.6 ± 11.9**

Figure 3 shows the relationships between 3D estimated measurements and L_M, the 1D gold standard measurement of tissue destruction that is the hallmark of emphysema. We observed that the ratio of airspace volume to total lung volume significantly correlated with L_M when evaluating both wildtype and elastase lung measurements. In addition, we also observed a modest but significant correlation between the ratio of tissue volume to airspace volume and L_M.

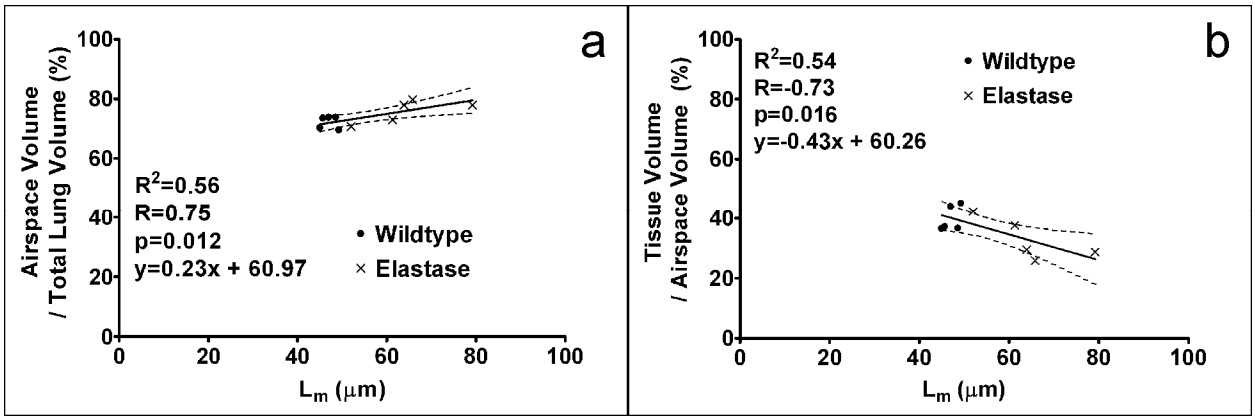

Figure 3. The significant relationship between (a) L_M and Airspace volume/Total lung volume and (b) L_M and Tissue volume/Airspace volume is shown for 5 mouse lobes, in a single wild-type and elastase mouse each.

New or Breakthrough work to be presented:

We developed a way to generate 3D histology volumes/images after registration of digital histology slide images with 2x2x15 μm resolution. The resultant image volumes allow for *ex vivo* 3D measurements that can be directly compared to stereology and to 3D macroscopic imaging of the same tissue *in vivo.*

Discussion:

Although there are limitations inherent in our approach related to spatial resolution in the z plane, and the limited number of samples we employed in the proof of concept demonstration, our approach provides a way to estimate 3D measurements of lung tissue on a regional basis. This is critically important because of the regional heterogeneity of lung tissue destruction in emphysema and all respiratory disease. This has made the development of structure-function models of the lung very difficult to develop, validate and test. We expect to continue to refine and develop the current approach to incorporate a number of different staining methods to enhance and increase the information content of the 3D volumes generated. We also showed modest but significant relationships between 3D measurements and 1D measurements that provides a foundation for improved regional analyses.

Conclusions:

Recent developments by Hogg and co-workers (3) have showed that destruction of the lung terminal bronchioles may precede emphysematous destruction of the lung parenchyma in smokers. These findings were made possible because micro-CT provided a way to generate 3D measurements, whereas stereology measurements of the same tissues showed no significant difference between

emphysematous and healthy lung. The techniques we developed for 3D histology visualization and quantification presented here will aid in advancing our ability to co-register macroscopic and microscopic imaging which in the case of COPD will help provide an understanding of pathogenesis and disease progression.

References:

(1) Nelder JA, Mead R. A Simplex Method for Function Minimization. The Computer Journal 1965 January;7:308-13.

(2) Otsu N. A Threshold Selection Method from Gray-Level Histograms. Systems, Man and Cybernetics, IEEE Transactions on 1979;9(1):62-6.

(3) McDonough JE, Yuan R, Suzuki M, Seyednejad N, Elliott WM, Sanchez PG, Wright AC, Gefter WB, Litzky L, Coxson HO, Pare PD, Sin DD, Pierce RA, Woods JC, McWilliams AM, Mayo JR, Lam SC, Cooper JD, Hogg JC. Small-airway obstruction and emphysema in chronic obstructive pulmonary disease. N Engl J Med 2011 October 27;365(17):1567-75.